

# ANALYSIS OF THE BACKSCATTERED ENERGY IN TERRESTRIAL LASER SCANNING DATA

Norbert Pfeifer<sup>a,\*</sup>, Bernhard Höfle<sup>a,b</sup>, Christian Briese<sup>a</sup>, Martin Rutzinger<sup>c</sup>, Alexander Haring<sup>a,b</sup>

<sup>a</sup>Institute of Photogrammetry and Remote Sensing, Vienna University of Technology, 1040 Wien, Austria

<sup>b</sup>Christian Doppler Laboratory “Spatial Data from Laser Scanning and Remote Sensing”

<sup>c</sup>alpS-Centre for Natural Hazard Management, Innsbruck and Institute of Geography, Innsbruck University, Austria  
(np, bh, cb, ah)@ipf.tuwien.ac.at, martin.rutzinger@uibk.ac.at

**KEY WORDS:** Terrestrial Laser Scanning, Calibration, Radiometry, Intensity

## ABSTRACT:

Terrestrial laser scanning provides a point cloud, but usually also the “intensity” values are available. These values are mainly influenced by the distance from sensor to object and by the object’s reflection properties. We demonstrate that it is possible to retrieve these reflection properties from the observed range and the intensity value. An experiment with targets of known reflectivity behaviour is described. Retrieving object reflectivity is also demonstrated for these targets in another experiment, which was not used to determine the functional relationship between range, reflectivity, and intensity. The Lidar equation describes the received optical power in terms of the emitted power, range, and target properties. Nonetheless, the intensity values do not follow this prescribed behaviour. Therefore, data driven approaches are used, allowing a better prediction of the observed intensity from the range and reflectivity of the targets. For a Riegl LMS-Z420i and an Optech ILRIS 3D these experiments were performed. Both scanners measure range by the travel time of a pulse. In our experiments, the reflectivity can be estimated from the laser scanning data with a standard deviation of 6% or better. This demonstrates the potential for retrieving material properties of natural surfaces, too.

## 1. INTRODUCTION

Obtaining geometrical information from terrestrial laser scanning (TLS) is an established surveying procedure (Grün and Kahmen, 2007, Fritsch, 2007) and used e.g. in cultural heritage recording and industrial plant reconstruction. The acquired point clouds, i.e. sets of xyz coordinates, are used to determine object surfaces by triangulation, surface fitting, or primitive instancing. Airborne laser scanning (ALS) is similar with respect to the data provided: the point cloud. Calibration of the ranging and scanning devices is an issue in the terrestrial (Lichti 2007, Nothegger et al., 2007, Reshetyuk, 2006) and the airborne case (Kager, 2006 and references therein). This allows obtaining high precision, well beyond 1:10000. Laser ranging uses energy emitted from the sensor for determining the range between sensor and object. It is retrieved by measuring the two-way travel time of the signal bounced back at the object. Beyond the run-time it is possible to measure the strength of the backscattered signal as well. Object properties like specular and diffuse reflection behaviour, absorption, and transmission influence the strength of this backscatter. The so-called “intensity” value is related to the power (amplitude) or energy of the returned signal.<sup>1</sup> With calibration it becomes possible to convert these intensity values into parameters related to the object surface. In ALS methods for radiometric calibration have been proposed (Briese et al. 2008, Höfle et al., 2007 and references therein). Independent thereof, these intensity values have been used in TLS applications, e.g. for orientation (Akca, 2007), manual inspection of trees (Aschoff et al., 2004), and rock face investigation (Rosser et al., 2007).

In this paper we want to show that a radiometric calibration is possible for terrestrial laser scanners as well. It builds on and

enhances previous work of our group (Pfeifer et al., 2007). The next section gives motivations for doing this research. This is followed by a section on the theoretical basis, discussing also issues of not strictly monostatic laser rangefinders. Thereafter we present our experiments, where a Riegl LMS-Z420i and an Optech ILRIS 3D were used<sup>2</sup>. The calibration results and the discussion follow in the subsequent chapters.

## 2. MOTIVATION

The overall aim is to extract more information than “only” the xyz point cloud from TLS. This becomes possible if influences on the loss of emitted energy in comparison to the detected energy can be grouped into those depending on the object and other influences, e.g. the distance from sensor to object. Not only absorption and reflection properties, i.e. the BRDF, but also the incidence angle of the measurement are counted in the following to the object properties.

In many monitoring circumstances the objects observed are known. One example is TLS for snow monitoring (Prokop, 2006) for research on and assessment of avalanche risk. In the work of Prokop it is also observed that under certain meteorological circumstances no range measurements are possible, actually referring to an energy level too low to be detected. Kaasalainen and Kukko (2007) advance this approach with a more physical approach. In (Rees, 2006) it is described how the grain size of snow and the snow temperature affect the backscatter strength. From the intensity values it should therefore, at least theoretically, be possible to reconstruct snow pack properties from the intensity values. Similarly, over wet sand in comparison to dry sand, backscatter strength is smaller.

For the relative orientation of TLS data acquired from different stand points Wendt and Heipke (2006) have proposed using the

<sup>1</sup> We use the term “intensity” in this paper, but there is not necessarily a unique physical interpretation for these intensity values by the different scanner producers.

<sup>2</sup> Much of this paper applies to phase-shift systems as well.

intensities. They suggested a  $1/r^2$  correction factor before using the intensity images in matching procedures. While this factor can be justified theoretically, our work shows that it may not be optimal. In any case, quality figures estimated in the matching process will measure more of the actual texture similarity and less of the device influences, if calibration methods are applied to the data in advance. Also the visual appearance of laser scanning intensity images can possibly be improved by applying calibration procedures.

The ranging precision depends on the amount of backscattered energy, as higher energy levels lead to a higher signal-to-noise ratio, because the background noise can be considered as constant. The question arises, how much of the ranging precision depends on distance and on object brightness.

Finally, studying the intensity values is a means of investigating the laser scanners as such and improves the understanding of the measurement process. In the airborne case, but also for terrestrial laser ranging, pulsed systems use the intensity values for correcting the raw travel-time observation. This correction may become as big as a decimeter (personal communication), and it is the original motivation for recording the intensity. This, but also noise behavior, may become relevant in geometric calibration procedures.

Not all of these hypotheses will be investigated within this paper, but they show that there is a potential for using the intensity values. Especially the possibility to infer reflectivity of targets which are i) planar and have ii) known reflectivity behavior will be investigated. This builds the base for the other items of the above list.

### 3. THEORY

#### 3.1 Model driven approach

The basic equation for describing the strength of the backscatter from an object surface is the Lidar (light detection and ranging) equation (Jelalian, 1992). It relates the emitted optical power  $P_E$  to the received optical power  $P_R$ .

$$P_R = P_E D_R^2 / (4\pi \beta_E^2 r^4) \sigma \eta_{\text{Atm}} \eta_{\text{Sys}} \quad (1)$$

The term  $\sigma$  is the backscattering cross section and is a product of the directional reflection strength ( $\rho_D$ ) and the area of the object.  $\beta_E$  is the beam divergence,  $r$  the range,  $D_R$  the receiving aperture diameter, and the  $\eta$ -terms describe atmospheric and system transmission. If the reflecting surface is larger than the laser footprint, then the object is called an extended target. This removes the beam divergence from the equation and introduces a  $1/r^2$  dependency of the emitted power as opposed to  $1/r^4$ .

$$P_R = P_E D_R^2 / (4r^2) \rho_D \eta_{\text{Atm}} \eta_{\text{Sys}} \quad (2)$$

This equation can be simplified further under the assumption, that the target is a perfect Lambertian reflector. In that case the backscatter strength depends on the (Lambertian) target reflectivity  $\rho$  and the angle of incidence  $\alpha$ .

$$P_R = \pi P_E \rho \cos(\alpha) / (4r^2) \eta_{\text{Atm}} \eta_{\text{Sys}} \quad (3)$$

Knowing the emitted and the received power, and having measured the range and intensity value, allows determining the product  $\rho \cdot \cos(\alpha)$ . For smooth surfaces the angle of incidence may be estimated from a local surface model, which can be obtained by surface fitting to the neighbouring points. In ALS this has already proven successful (Höfle and Pfeifer, 2007).

The above equations furthermore idealize the emitter-receiver configuration and therefore are not valid in close proximity of the sensor itself. The beam profile is more complex, too. It is minimal at the beam waist and a linear increase of the footprint is only given at larger distances (Young, 2000).

In addition, emitter and receiver are assumed to be coaxial as in a strictly monostatic system. To avoid optical cross talk, emitter and detector are often separated (Ingensand, 2006). Thus, different fields of view (FoV) of detector and emitter have to be considered. Their opening angle and their direction can be different, and (see above) there is a small “base” between them. Depending on the i) geometrical configuration and the ii) range, the visibility of the beam footprint for the detector may run through the following stages: not visible - partly visible - fully visible - partly visible - not visible. This effect is overlaid to the  $1/r^2$  decrease of received energy. A simplified simulation is shown in Fig. 1. As it is demonstrated the received energy starts increasing with increasing range, because more and more of the footprint gets into sight. For larger ranges it starts decreasing again, because most of the footprint is visible already, and the decay of received power with  $1/r^2$  is stronger. An in-depth discussion of this “form factor” can be found in Riegl and Bernhard (1974) and Stelmasczyk et al. (2005).

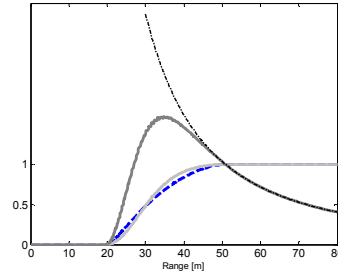


Figure 1: Simplified simulation of the effect of partly overlapping footprints. Beam diameter at exit: 3mm, beam divergence: 0.35mrad. The beam energy is distributed according to a Gaussian bell curve, and no energy is assumed to be outside of the circle where the energy drops to  $1/e^2$ . Base between emitter and receiver centre: 3cm, parallel axes, detector diameter: 3cm, opening angle: 1mrad. The dashed curve shows the portion of the visible footprint in the detector FoV. The solid light gray line shows the portion of footprint energy visible in the detector FoV. The footprint starts getting into sight at a range of 20m and is fully visible from 50m onwards. The thin, dash-dotted black curve shows the theoretical  $1/r^2$  decay of received power according to Eq. (1), and the dark gray curve the combined effect.

The effects of beam waist, detector aperture, and base, can be considered, provided these parameters are known. Servicing of the device may lead to new values, and long term stability may not necessarily be given. Additionally, these parameters may not be disclosed by the device manufacturers. Also estimating these parameters requires knowledge of the system design.

So far, the relation of emitted to received optical power was discussed. The received signal is usually converted to an electrical signal and amplified by an APD (avalanche photo diode) and then digitized. This amplification is not necessarily linear, and frequently a logarithmic behaviour is assumed. Furthermore, for round-trip-time systems the emitted pulse is not a Dirac impulse but has a duration in the order of a few ns, e.g. 5ns, corresponding to a pulse length of 1.5m. The “intensity” may refer to the maximum, the average below the pulse shape, or the energy level after a certain amount of time.

It does stand to reason to evaluate alternative approaches, relating intensity values, ranges, and target reflectivity to each other without considering the physical foundation.

### 3.2 Data driven approach

In the previous section it has been shown that a number of unknown system parameters may exist. This complicates using a model driven approach, because the system parameters need to be known for estimating object properties, especially object cross section  $\sigma$  or object reflectivity  $\rho \cdot \cos(\alpha)$  for Lambertian targets, from the observed range  $r$  and intensity  $I$ .

In a data driven approach the function  $f$  is determined. In a general case, but restricted to Lambertian targets, it can be written as  $f(r, I, \alpha, \rho) = 0$ . From a set of observations and corresponding known object properties the parameters of  $f$  can be estimated. For typical data from laser scanners  $r$  is determined more precisely, with a coefficient of variation<sup>3</sup> below 1%, whereas the intensity value has a coefficient of variation of 3% to 10% (Pfeifer et al., 2007, Höfle and Pfeifer, 2007). It therefore stands to reason to choose  $r$ ,  $\rho$ , and  $\alpha$  as function parameters, because they are determined more precisely, than the function value  $I$ . This allows formulating residuals  $e_I$  in an observed quantity.

$$I + e_I = g(r, \rho, \alpha) \quad (4)$$

The function  $g$  should fulfil the following requirements. Firstly, it should explain the data well. The  $I$  should have small residuals:  $e_{Ij} = g(r_j, \rho_j, \alpha_j) - I_j$ , for sets of data quadruples with  $j=1, \dots, n$ , ( $n$  the number of points). The standard deviation  $\sigma_0$  of the residuals<sup>4</sup>, obtained from a function  $g$  with  $u$  parameters can be used to judge the explanatory power of  $g$ .

$$\sigma_0 = (\sum e_{Ij}^2 / (n - u))^{0.5} \quad (5)$$

Secondly, the function  $g$  should not contradict basic physical principles. As details of the device model are unknown, this is limited. However, the parameters  $\rho$  and  $\alpha$  of the object have similar effects on the backscattered power, namely decreasing it for smaller values of  $\rho$  and larger values of  $\alpha$ . The beam diameter is small, in the order of a few mm, whereas the pulse length for a round-trip-time measurement system is in the order of meter. Thus, the stretching of the pulse may be neglected, too<sup>5</sup>. The effects of  $\rho$  and  $\alpha$  may therefore be bundled to  $k = \rho \cdot \cos(\alpha)$ , which is in line with the basic physical principles.

Thirdly, the function should avoid effects not observed in the data. Properties like monotonic behaviour or smoothness, which are visually apparent in the data, should also be properties of the function  $g$ . A decreasing series of values strictly interpolated by a polynomial may give rise to an oscillatory function, which cannot be justified by the data. With an increasing number of parameters  $u$  the function  $g$  may also start modelling the noise. The noise would be different in a repetition of the experiment and should not be represented by  $g$ .

Finally, the function should be invertible. This is necessary for uniquely finding the reflectivity given observations of  $r$  and  $I$ .

<sup>3</sup> The coefficient of variation is standard deviation / mean.

<sup>4</sup> N.B.:  $\sigma$  now refers to a quality measure, and not to the scattering target cross section, introduced in section 2.

<sup>5</sup> Assuming a pulse with constant distribution of power across and along the beam, a 5mm spot size, a target inclination of 45°, and a 4ns pulse duration (1.2m), this stretch is below 1%.

The following types of functions are possible, of which especially the nested approach will be investigated.

- Separation approach:  $I = g_1(r) * g_2(k) + g_3$
- Nested approach:  $I = g_4(k, g_5(r))$
- Surface fitting approach:  $I = g_6(r, k)$

Next to  $\sigma_0$  also  $\sigma_r$  will be used to judge the distribution of residuals. The term  $\sigma_r$  refers to the root mean square value of the residuals, and is different from  $\sigma_0$  by the denominator under the root.

## 4. EXPERIMENT

Reference targets with known reflectivity behaviour were used. These targets are made of Spectralon®, which reflects according to a Lambertian scatterer (cosine-law). The targets are quadratic with an edge length of approximately 13cm, and mounted onto a metal frame, holding all six targets with reflectivities of about 5%, 20%, 40%, 60%, 80%, and 99%. The frame was placed in different distances to the laser scanners and at different aspects. Points measured on one target were selected, and for the point set of each target at each range and aspect, a number of parameters was determined. Also, a plane was fitted to the points minimizing the orthogonal distances. This allows computing further parameters. Finally, for each target the following parameters were used (Table 2).

$\rho$ [ ]	Target reflectivity
$\alpha$ [°]	Mean angle of incidence (to the plane)
$r$ [m]	Mean range
$I$ [ ]	Mean observed intensity value

Table 2: Parameters determined for each target in the experiments. Symbols are given with their units.

Scanning was performed with a Riegl LMS-Z420i (termed Riegl) and an Optech ILRIS 3D (termed Optech). For each device, two series of measurements were performed. In the first series the distance of the target frame to the scanner was changed: up to 15m in 1m-steps, thereafter in 5m steps, up to the maximum length of the laboratory (50m). In the second series the target frame was placed at a distance of approximately 15m to the scanner, and rotated in 9° steps from 0° to 72°.

The Riegl scanner operates at a wavelength of approximately 1550nm. At this wavelength the reflectivity of the targets are 0.986, 0.828, 0.653, 0.433, 0.233, and 0.081.

For the distance series the minimum and the maximum mean range were 2.02m and 50.04m, and mean intensities varied from 0.1207 to 0.3085. The maximum angle of incidence was 11.4° for the target on the outer end of the frame at the shortest distance. By the cosine-law this corresponds to a decrease of return energy of 2% (see Eq. (3)).

For the angle series the minimum and maximum distance were within 14.89m and 15.15m<sup>6</sup>, originating in the rotation of the target frame. The largest angle of incidence for which the targets could be extracted from the measured data was 72.0°, which corresponds by the cosine-law to a decrease by 69%. The average intensities varied between 0.1156 and 0.1880.

The Optech scanner operates at a wavelength of approximately 1540nm. At this wavelength the reflectivity of the targets are 0.986, 0.827, 0.653, 0.433, 0.233, and 0.080. For the distance

<sup>6</sup> From the analysis performed thereafter, this range difference has an influence of 3% on the intensities.

series the minimum distance, at which measurements were recorded was 3.98m. No distances could be measured at the 3m step. The maximum incidence angle in this series is  $4.5^\circ$ , corresponding by the cosine-law to a decrease in return energy by 0.3%. The average intensities are between 0.0065 and 0.2462. Originally, the values were up to 5 digit integers, but to make them comparable to the Riegl data they were scaled by setting the maximum single intensity in the entire data set to 1.

For the series of measurements at different incidence angles, the ranges were between 14.84m and 15.09m.<sup>7</sup> Data from incidence angles up to  $71.9^\circ$  could be retrieved, corresponding by cosine to 0.311, i.e. a decrease in intensity by 69%. The averaged intensities for the individual targets are between 0.0089 and 0.2138.

Data of the range experiments is shown in Fig. 3.

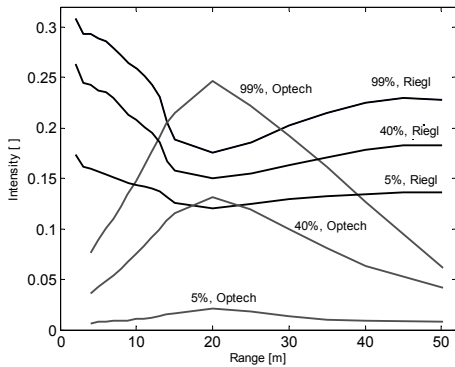


Figure 3: Mean intensities for the Riegl and the Optech laser scanner for three targets (99%, 40%, and 5% reflectivity) at different distances.

## 5. RESULTS

### 5.1 Modelling with the Lidar equation

If the Lidar equation shall be used for modelling the intensity values, it is obvious that it can only apply to a selected range interval. For the Optech data this applies to the ranges above 30m, thus for the experiments shown in the interval [30m,50m]. This is also suggested by Larsson et al. (2006). However, this approach is not pursued because of the obvious limitations.

### 5.2 Separation approach

The separation approach was investigated previously in Pfeifer et al. (2007). As is shown below, other approaches allow higher precision, and therefore the presentation of results will be very limited. It is interesting, however, to compare the results obtained now to previous investigations.

In 2007 experiments with the same Riegl scanner as used in this study, i.e. the same physical device, were performed, using a similar setup of measurements. The main difference is, that the angle experiment was performed at a distance of 5m. For the data acquired now, the following functions were determined by optimization in the separation approach:

$$g_1(r) = \begin{cases} r < 15m: & g_1(r) = -0.0082r + 0.3338 \\ r > 18m: & g_1(r) = 0.0019r + 0.1441 \end{cases} \quad (6)$$

$$g_2(p \cdot \cos(\alpha)) = g_2(k) = k^a, \text{ with } a = 0.22, g_3 = 0$$

The influence of the range in  $g_1$  is described by a piecewise linear function, first decreasing and then increasing with range. A smooth transition between the two intervals is added. The function  $g_2$  is an exponential function, and  $g_3$  identical to zero as in the previous study.

The distribution of the residuals is characterized by  $\sigma_r = 0.0114$  for all observations, separated for the range and the angle experiment into  $\sigma_r = 0.0080$  and  $\sigma_r = 0.0167$ , respectively. The mean values of the distribution are 0.0 and 0.0078.

### 5.3 Nested approach

The nested approach takes the form  $I + e_l = g_4(k, g_5(r))$ . The function  $g_5$  depends on the range only, but it determines one or several parameters of the function  $g_4$ . These parameters are e.g. polynomial coefficients. In that case,  $g_5$  is a vector valued function. Specifically, the following form was used in this study.  $g_4$  is a cubic polynomial, and  $g_5$  is a vector-valued function in 4D, determining the coefficients of  $g_4$ . Precisely put,  $g_5$  is a vector valued 3<sup>rd</sup> order polynomial. This describes a Bi-Cubic Tensor-Product surface patch (Farin, 2002).

For increasing flexibility, multiple patches can be laid out in the parameter domain  $(r, k)$ , joining with suitable continuity conditions. For the data acquired with the Riegl and the Optech instrument, two patches were used, splitting the interval of  $r$ , similar as in the separation approach. Strict continuity was not enforced, but reached approximately.

For the Riegl data the patch border is at  $r=15m$ . This split was obvious when looking at the curves of intensity vs. range (Fig. 3). For estimating the functions, however, first the measurements to the six targets were analysed independently per distance step.

For each distance step the data of mean target intensity  $I$  over  $k = p \cdot \cos(\alpha)$  was analysed. As this approach is formally expressed as  $I = g_4(k, g_5(r))$ , this means that at fixed values of  $r$  the function  $g_4$  could be fitted to the data. Different models were used for this, but for the clarity of the explanation only the cubic polynomial is considered. As six targets were available, this means that an overdetermination of two was available for the cubic fit. In Figure 4 the cubic polynomials together with the data are shown for all distance steps. The coefficients are shown in Figure 5.

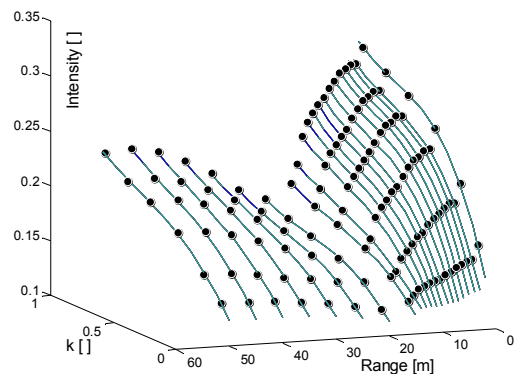


Figure 4: Data of the Riegl distance experiment series. Each bullet represents the data of one target at a certain range and  $k$  (product of reflectivity and cosine of incidence angle). The vertical axis is the mean intensity per target. Targets are grouped by distance, and for each distance the least squares fit 3<sup>rd</sup> order polynomial is shown.

<sup>7</sup> The previous footnote does not only apply to the Riegl device but also to the Optech device.

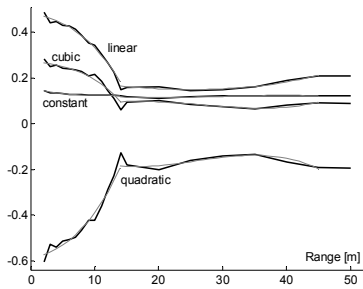


Figure 5: Polynomial coefficients (fat black lines) of the functions of Figure 4, i.e. cubic polynomials in the monome form. These polygons are approximated by cubic polynomials each (thin gray lines), split for ranges below and above 15m.

Experiment series	$g_4$ -Model	$\sigma_0$ abs., $\sigma_0$ rel.	$\sigma_r$	
Distance	Cubic	0.00297, 1%	0.00255	
Distance	Log.	0.00659, 2%	0.00614	
Angle	Cubic		0.00241	5% better
Angle	Log.		0.00656	7% worse

Table 6: Precision values for the different data driven models ( $2^{\text{nd}}$  col.) of the Riegl data. “ $\sigma_0$  abs.” is the a-posteriori precision (Eq. 5), and “ $\sigma_0$  rel.” is the portion of  $\sigma_0$  on the maximum mean target intensity. The  $4^{\text{th}}$  col. shows the r.m.s. of the residuals, and the results can be compared between the distance experiment, used for parameter estimation, and the angle experiment ( $5^{\text{th}}$  col.).

The coefficients of the cubic polynomials for each distance step can also be regarded as discrete observations of curves: one curve for the constant term, one for the linear, etc. The vertices of these curves can again be used for fitting a curve model. If a cubic polynomial is chosen, then the resulting patch is bi-cubic.

- For  $g_4$  not only cubics, but the following functions were tested.
- Logarithmic function, with constant offset and scale factor. This is suitable, if the conversion from optical to electronic power is a logarithmic amplification.
  - Linear scaling, suitable if received optical power and intensity value are directly proportional, termed “Scale” below.
  - Linear function: like “Scale”, but adding a constant offset, e.g. background noise.
  - Cubic polynomial, providing flexibility but still over-determination in the estimation procedure.

For  $g_5$  always cubic polynomials were used, as the data does not follow the Lidar equation (Figure 3). However, some similarity of the Optech data to the curve shape of Figure 1 can be noted.

Next, the results of the different models will be presented. Only those models describing the data reasonably well are presented. Also the Optech data had to be split into two patches for ranges above and below 18m. As it can be seen in Fig. 5, the data cannot be approximated well for the last distance step (50m). These measurements were excluded from further analysis.

The model is determined from the range series as explained. The angle series can then be used to verify the suitability of the model. It should be kept in mind, that the mean intensity values of the Riegl angle experiment data drop below the lowest mean intensities of the distance experiment (0.1156 vs. 0.1207). Thus, there is a certain amount of extrapolation with respect to  $k$ . For the Optech data this is not the case. The Riegl results are summarized in Table 6, the Optech results in Table 7.

Experiment	$g_4$	$\sigma_0$ abs., $\sigma_0$ rel	$\sigma_r$	
Distance	Cubic	0.00218, 1%	0.00180	
Distance	Linear	0.00613, 3%	0.00508	
Distance	Scale	0.00681, 3%	0.00564	
Angle	Cubic		0.00814	452% worse
Angle	Linear		0.00716	41% worse
Angle	Scale		0.00765	36% worse

Table 7: Precision values for different data driven models for the Optech data. Columns as in Table 6.

## 6. DISCUSSION

With the data acquired in the previous experiment (Pfeifer et al., 2007) with the Riegl scanner the precision  $\sigma$  was 0.0108. The precision obtained now for the separation approach is comparable and approximately worse by 10%. The parameters also changed, which is attributed to the new data distribution in the experiments. Nonetheless, the behaviour of the device, namely decrease and increase of intensity depending on the range with a minimum at  $\sim 15\text{m}$  was the same. The precision obtained with the new data driven approaches are much higher and the separation method will not be discussed further.

The two scanners show different, i.e. opposite, behaviour of intensity vs. range. Both deviate strongly from the pure Lidar equation, showing that it does not hold for the distances investigated. To reach a better agreement the model would have to be extended, depending on the system design. The effect of overlapping footprints, simulated in Sec. 3, appears to be similar to the function shown for the Optech scanner in Figure 3. For the Riegl scanner the situation is more complicated, and currently we do not have a good explanation. However, this behaviour was also found in Pfeifer et al. (2007) and the stability of the device could be confirmed.

The nested models all produce satisfying results concerning the data of the range experiments. The mean intensity can be predicted with a precision of 1% for both scanners.

For the Riegl scanner a bi-cubic model was found to provide best results. For each range the intensity is described as a cubic polynomial of the product of target reflectivity and cosine of the incidence angle. This function can be seen as the transfer (amplification) function from optical power to the digital intensity values. In all the experiments this function proved to be strictly monotonously growing. It is, therefore, invertible, allowing to infer reflectivity from range and intensity. Also, no oscillatory behaviour could be detected. The model is therefore suitable and fulfils the requirements of Sec. 3.2. For the Optech scanner, the cubic model is best for the range experiment.

Concerning the angle experiment, the prediction is different for the two scanners. Testing the model for the Riegl scanner is an extrapolation, as lower mean intensities were obtained than in the range experiments. Still, the estimation of the intensity on the basis of the known reflectivity and the estimated incidence angle was possible with the same accuracy. This confirms that the model proposed fits well to the data and its temporal stability should be investigated next. For the Optech data the intensity in the angle experiments can be predicted not as good.

While predicted intensities can be compared to observed ones, it has more applications to estimate the reflectivity  $\rho_E$  (or  $k$ , the target cross section, ...) from the intensities. As noted above, for a given range  $r$   $g_4$  is always monotonous and thus invertible.

In Table 8 the distribution of estimated reflectivity residuals  $e_p$ ,  $= \rho - \rho_E$ , computed from mean range, incidence angle, and intensity, is shown. It should be considered that the model parameters were derived from the range experiment and then also applied to the angle series to evaluate these parameters.

experiment	$g_4$	mean $e_p$	std. $e_p$	min., max. $e_p$
Riegl, range	Cubic	0.0004	0.0271	-0.0699, 0.0897
Riegl, angle	Cubic	0.0026	0.0549	-0.1628, 0.1089
Riegl, range	Log.	-0.0221	0.1273	-0.5412, 0.1209
Riegl, angle	Log.	0.0291	0.1325	-0.3442, 0.2273
Optech, range	Cubic	-0.0001	0.0119	-0.0278, 0.0298
Optech, angle	Cubic	0.0234	0.0609	-0.1069, 0.2028
Optech, range	Linear	0.0000	0.0277	-0.0582, 0.0419
Optech, angle	Linear	0.0204	0.0469	-0.0568, 0.1600
Optech, range	Scale	-0.0046	0.0287	-0.0696, 0.0526
Optech, angle	Scale	-0.0072	0.0466	-0.1012, 0.0851

Table 8: Residuals of reflectivity estimated from  $r$ ,  $\alpha$ , and  $I$ .

For the Riegl data it holds that the cubic model fits much better for the inverse task than does the logarithmic model. Also, the extrapolation to low intensity values observed in the angle experiment obviously has a more severe influence. For the given distance range of [2m,45m] the reflectivity of smooth surfaces can, however, be estimated from the range and intensity data with a systematic error of 2% and a standard deviation of 6%. This assumes that the angle of incidence can be estimated precisely. The numbers for the estimation of  $k$  are similar. With the approach of Pfeifer et al. (2007) this inversion was possible with a standard deviation of 23% only.

For the Optech data the values of the cubic model are similar to those of the Riegl data. However, the other two models fit also comparably good. For the angle experiment the linear and the scale model fit even better, and thus should be used for the inversion. In the distance range of [4m,40m] the reflectivity of smooth surface can, therefore, be estimated from the range and intensity data with a systematic error of maximum 2% and a standard deviation of 5%.

## 7. CONCLUSIONS

The purpose of terrestrial laser scanners is currently mainly in acquiring geometry. It was shown that the intensity values provided alongside the range are not realizations of the Lidar equation in its simple form (Eq. 1, Eq. 3). The inherent assumptions (coaxial system, etc.) do not hold. However, the components of these laser scanners work consistently and allow reconstructing also target properties like reflectivity, if the scattering properties are known. It was shown that this is possible in the range of the shortest measurable distances to approximately 50m for the specific devices used, namely a Riegl LMS-Z420i and an Optech ILRIS 3D. The reflectivity of Lambertian targets could be reconstructed with a precision of about 6% and a bias in the order of 2%. This demonstrates the great potential for using these devices in monitoring applications, where the backscatter strength depends on material properties. Laser scanning should therefore be considered a 4D measurement process, with each coordinate holding object information.

The standard deviation of the intensity values and the plane fit results should be analysed next. Also, larger distances should be investigated. Likewise, the temporal stability of the function parameters has not been studied. Verifying the stability would allow calibrating once, with no need to use the reference targets

for subsequent applications/experiments of the intensity values. Finally, also the properties of phase shift scanners should be studied with respect to "their" intensity values. Eventually, under the assumption that the "increasing intensity with range" behaviour originates in the changing overlap of emitter and receiver field of view, also the energy distribution within each footprint becomes important and should be investigated. The final aim is, of course, verifying the findings over natural surfaces.

## ACKNOWLEDGMENTS

Part of this project was supported by the Vienna University of Technology innovative project "The Introduction of ILScan technology into University Research and Education". We are especially grateful to M. Vetter for the experiment support.

## REFERENCES

- IAPRS = Int. Archives of Photogrammetry and Remote Sensing  
 ISPRS-J = ISPRS Journal of Photogrammetry and RS
- Akca, 2007. Matching of 3D surfaces and their intensities. ISPRS-J, 62.
- Aschoff, Thies, Spiecker, 2004. Describing forest stands using terrestrial laser-scanning. IAPRS 36, 8/W2, Freiburg, Germany.
- Briese, Höfle, Lehner, Wagner, Pfennigbauer, Ullrich, 2008. Calibration of full-waveform airborne laser scanning data for object classification. SPIE 6950, Laser Radar Technology and Appl. XIII.
- Farin, 2002. Curves and Surfaces in CAGD (5<sup>th</sup> ed). Academic Press.
- Fritsch (Ed.), 2007. Photogrammetric Week '07, Wichmann.
- Grün and Kahmen (Ed.), 2007. Proceedings of the VIII conference on Optical 3D Measurement Techniques.
- Höfle and Pfeifer, 2007. Correction of laser scanning intensity data: Data and model-driven approaches. ISPRS-J 62(6).
- Ingensand, 2006. Metrological aspects in terrestrial laser-scanning technology. 3rd IAG / 12th FIG Symposium.
- Kaasalainen and Kukko, 2007. Snow Reflectance Measurements using terrestrial Laser Scanner. Geophysical Research Abstracts 9(02755).
- Kager, 2006. The Importance of Exact Geo-referencing of Airborne LIDAR Data. Natural Resource Management: Going Critical, 10(4).
- Larsson, Steinvall, Chevalier, Gustafsson, 2006. Characterizing laser radar snow reflection for the wavelengths 0.9 and 1.5  $\mu\text{m}$ . Optical Engineering 45(11).
- Lichti, 2007. Error modelling, calibration and analysis of an AM-CW terrestrial laser scanner system. ISPRS-J. 61(5).
- Nothegger and Dorninger, 2007. Automated Modeling of Surface Detail from Point Clouds of Historical Objects. IAPRS 36, 5/C53.
- Pfeifer, Dorninger, Haring, Fan, 2007. Investigating terrestrial laser scanning intensity data: quality and functional relations. Proc. of VIII conference on Optical 3D measurement tech.
- Prokop, 2006. Determination of spatial snow depth distribution using terrestrial laserscanner. 9th International Symposium on High Mountain Remote Sensing Cartography, Graz.
- Rees, 2006. Remote Sensing of Snow and Ice. CRC Press.
- Reshetyuk, 2006. Calibration of terrestrial laser scanners for the purposes of geodetic engineering. 3rd IAG / 12th FIG Symposium.
- Riegl and Bernhard, 1974. Empfangsleistung in Abhängigkeit von der Zielentfernung bei optischen Kurzstrecken-Radargeräten. Applied Optics 13(4).
- Rosser, Sunning, Petley, 2007. Multi-spectral terrestrial laser scanning for interpreting the controls on and changes to unstable rock faces. Geophysical Research Abstracts 9(07021).
- Stelmaszczyk, Dell'Aglio, Chudzynski, Stacewicz, Wöste, 2005. Analytical function for lidar geometrical compression form-factor calculations. Applied Optics 44(7).
- Wendt and Heipke, 2006. Simultaneous orientation of brightness, range and intensity images. IAPRS 36, 5.
- Young, 2000. Optics and Lasers, 4<sup>th</sup> ed. Springer.